Uniform, luminescent Eu:LuF_3 nanoparticles.

Ana I. Becerro,[*] *Daniel González-Mancebo, Manuel Ocaña*

Instituto de Ciencia de Materiales de Sevilla (CSIC-University of Seville).
c/ Américo Vespucio, 49. 41092 Seville (Spain).

[*] Corresponding author. E-mail address: anieto@icmse.csic.es. Tel no: +34 95448945. Fax no: 954460165

Abstract

A simple procedure for the synthesis orthorhombic, uniform, LuF_3 particles with two different morphologies (rhombus- and cocoon-like) and nanometer and sub-micrometer size, respectively, is reported. The method consists in the aging, at 120ºC for 2 h, a solution containing [BMIM]BF_4 ionic liquid (0.5 mL) and lutetium acetate (in the case of the rhombi) or lutetium nitrate (in the case of the cocoons) (0.02 M) in ethylene glycol (total volume 10 mL). This synthesis method was also adequate for the synthesis of Eu^{3+}-doped LuF_3 particles of both morphologies, whose luminescence properties were investigated in detail. The experimental observations reported herein suggest that these materials are suitable phosphors for optoelectronic as well as in-vitro biotechonological applications.

Keywords: LuF_3, nanoparticles, ionic liquid, luminescence, concentration quenching.

Introduction

Lanthanide-doped rare earth (RE) fluoride matrices such as REF_3 and $NaREF_3$ have become a research focus in the optical materials field owing to their unique applications in optical telecommunication, lasers, and biochemical probes (Downing et al. 1996; Yi et al. 2004; Wang et al. 2006). In comparison with oxygen-based systems, fluorides possess very low vibrational energies and therefore the quenching of the excited states of the lanthanide ions is minimal (Diamente et al. 2007). In addition, RE fluorides exhibit high thermal and chemical stability, which make them ideal for luminescent purposes. It is highly desirable, for many of the mentioned applications, to have uniform nano- or submicron- particles with controlled size and shape, as well as good dispersion (Yi et al. 2004; Wang et al. 2006; Sun et al. 2007).

A number of highly monodisperse, nanometer and submicrometer size YF_3, LaY_3 and GdF_3 particles have been reported in the literature with very promising results for their use as both upconversion and down conversion phosphors (Mai et al. 2006; Wang et al. 2007; Rao et al. 2014; Carniato el at. 2013). However, fewer reports can been found on the synthesis of uniform Lu-based fluoride hosts in spite of their excellent luminescence and even better laser performance than their Y-based counterparts (Maunier et al. 2002; Sudesh and Asai, 2003; Liu et al. 2011; Li et al. 2011). In particular, most papers published about the synthesis of LuF_3 report either heterogeneous, polydisperse sub-microparticles (Xiao et al. 2007; Li et al. 2008; Lin et al. 2013) or aggregated nanoparticles (Qiu et al. 2014). Only Li et al. (2008) reported a synthesis method adequate to obtain uniform LuF_3 particles of micrometer-sized. In all these cases, the synthesis methods used involve either relatively high temperatures ($\geq$ 180 ºC) or/and the use of toxic surfactants (DDBAC) or complexing agents (EDTA).

Herein, we report a really simple (it does not require the use of toxic additives) low temperature (120ºC) route for the synthesis of uniform LuF_3 particles, through controllable release of F^- anions from an ionic liquid, with two different morphologies (rhombus- and cocoon-like shape) and narrow size distribution. We have investigated the influence of different Lu and F precursors, their concentrations, solvents, aging temperature and heating method on the morphology of the synthesized particles. The same method used to obtain uniform LuF_3 particles has also been successfully applied

to obtain Eu^{3+}-doped LuF_3 particles of both morphologies, whose luminescence properties have been investigated in detail.

Experimental section

1. Synthesis of samples

The procedure for the synthesis of the particles was as follows. Rhombus-like LuF_3 particles were obtained using lutetium acetate hydrate (0.02 M $Lu(CH_3COO)_3 \cdot xH_2O$, Sigma Aldrich, 99.9%) as the lutetium source, while lutetium nitrate hydrate (0.02 M $Lu(NO_3)_3 \cdot xH_2O$, Sigma Aldrich, 99.99%) was necessary for the synthesis of cocoon LuF_3 particles. In both cases, the lutetium salt was added to ethylene glycol (EG, $C_2H_6O_2$, Fluka, 99.5%), keeping magnetic stirring and heating at 70 ºC to favor dissolution. The solutions were then cooled down to room temperature and admixed with 0.5 cm^3 of 1-butyl-2-methylimidazolium tetrafluoroborate ([BMIM]BF_4, $C_8H_{15}BF_4N_2$, Aldrich ≥ 97 %). After homogenization, the final solutions (total volume = 10 cm^3) were aged for 2 h in tightly closed test tubes using an oven preheated at 120 ºC. The resulting dispersions were cooled down to room temperature, centrifuged to remove the supernatants and washed, twice with ethanol and once with double distilled water. For some analyses, the powders were dried at room temperature. The Eu^{3+}-doped particles were synthesized with the same procedure using Eu^{3+} acetate hydrate ($Eu(CH_3COO)_3 \cdot xH_2O$, Sigma Aldrich, 99.9%) and Eu^{3+} nitrate hydrate ($Eu(NO_3)_3 \cdot xH_2O$, Sigma Aldrich, 99.9%) in stoichiometric amounts. The lanthanide ions (Lu + Eu) concentration was kept constant (0.015 $mol \cdot dm^{-3}$) in all experiments, whereas the Eu/(Lu + Eu) molar ratio was varied from 0.5% to 40% in order to investigate the effect of this parameter on the morphological and luminescent properties of the precipitated particles.

2. Characterization techniques

The shape and size of the particles was examined by both *transmission electron microscopy* (TEM, Philips 200CM) and scanning electron microscopy (SEM-FEG Hitachi S4800). Particle size distributions were obtained from the micrographs by counting several hundreds of particles. Additional information on the size and colloidal stability of the particles in aqueous suspension (0.5 $mg \cdot mL^{-1}$ of solid) was obtained

from *Dynamic Light Scattering* (DLS) measurements. The experiments were carried out using a Malvern Zetasizer Nano-ZS90 equipment, which was used as well to measure the zeta potential of the suspensions.

The crystalline structure of the prepared particles was assessed by *X-ray diffraction* (XRD) using a Panalytical, X´ Pert Pro diffractometer (CuKα) with an X-Celerator detector over an angular range of $10º < 2\theta < 70º$, 2θ step width of 0.05º, and 10 s counting time. The crystallite size was calculated using the Scherrer formula from the full width at half maximum of several single reflections. Unit cell parameters of the undoped and the Eu^{3+}-doped particles were calculated from the XRD patterns using the Rietveld method with the TOPAS software. Starting crystallographic parameters were taken from those reported for orthorhombic LuF_3 in ICDD PDF 00-032-0612. Nominal Eu^{3+} contents were added to the structure. Refined parameters were: scale factor, zero error, background coefficients, unit cell parameters and atomic coordinates and atomic displacement factors of the lanthanide atoms.

The *infrared spectra* of the powders, diluted in KBr pellets, were recorded in a Jasco FT-IR-6200 Fourier transform spectrometer.

Finally, the *excitation and emission spectra* of the Eu^{3+}-doped LuF_3 particles, dispersed in water (2.5 $mg \cdot mL^{-1}$), were measured in a Horiba Jobin Yvon spectrofluorimeter (Fluorolog3). The emission spectra were transformed to the CIE color coordinates system using a 2º observer.

Results and discussion

It is well known that uniform particles can be obtained by precipitation through a slow and controlled release of the precipitating anions or cations in the reaction medium (Matijevic, 1993). We have used, in the present study, a strategy based on the controlled release of fluoride anions using an ionic liquid ($[BMIM]BF_4$) as fluoride precursor and two different lutetium salts (lutetium acetate hydrate and lutetium nitrate hydrate), which provide different particle morphology. The required fluoride anions are liberated by the ionic liquid as a consequence of its hydrolysis with the hydration water molecules of the lutetium precursor (Jacob et al. 2006). Ionic liquids are non-volatile, non-flammable and thermally stable organic salts with low melting point, which show a

superior capability for the solvation and stabilization of metal ions, which gives to them the possibility of acting as capping agents or surfactants. Ethylene glycol (EG) was selected as solvent because polyols have been amply shown to be suitable solvents for the synthesis of nanomaterials, as they may act not only as solvent but also as capping agent, thus limiting particle growth (Feldmann, 2003).

1. Morphology, colloidal stability and crystal structure of the precipitated LuF_3 particles.

Figure 1 (top) shows the TEM micrographs of the particles obtained after aging, at 120 ºC in a conventional furnace for 2 hours, a solution containing lutetium acetate (0.02 M) and [BMIM]BF_4 in EG. Using the same experimental conditions but changing the lutetium source to lutetium nitrate (0.02 M) led to the particles shown in the TEM micrographs of Figure 1 (bottom), which only needed 30 minutes aging to reach their final morphology. These experimental conditions allowed the synthesis, in both cases, of particles, homogeneous in both shape and size, and with a high degree of dispersion. The morphology of the particles is shown in detail in the insets of each of the TEM micrographs. As observed, using lutetium acetate as the lutetium source led to the synthesis of rhombus-like particles with two rounded and two sharp vertices. Their long axis length was ~180-200 nm (standard deviation = 30) while the short axis length was ~100 nm (standard deviation = 20). However, when lutetium nitrate was used as the lutetium precursor, cocoon-like particles (300 (30) nm x 150 (20) nm) were obtained.

Although the TEM micrographs shown in Figure 1 suggested that the particles were uniform and non-aggregated, this aspect was further confirmed by dynamic light scattering (DLS) measurements conducted on an aqueous suspension of both types of particles (pH 6.8). The average hydrodynamic diameter obtained by DLS was 190 nm for the rhombus-like particles and 220 nm for the cocoons (Figure 2). These data confirm the absence of particles aggregation and reveal that the particles are stable in an aqueous medium at close to neutral pH. The zeta potential values calculated on the same suspensions were 46.9 mV and 46.3 mV for the rhombus- and cocoon-like particles, respectively, which suggest that the colloidal stability of the suspensions was mainly due to the electrostatic repulsion among positively charged particles.

The crystalline structure of both types of the precipitated particles was assessed from their X-ray diffraction patterns (Figure 3, top). Both patterns match the standard PDF

ICDD 00-32-0612 corresponding to LuF_3, indicating that in both cases the LuF_3 particles exhibit an orthorhombic symmetry with space group *Pnma*. The width of the reflections is clearly different from one pattern to the other, the cocoon particles showing the wider reflections. As a consequence, the crystalline domain size in the cocoon particles (calculated using the Scherrer formula on single reflections) was of 10 nm while that of the rhombus-like particles was of 15-20 nm. If one compares these values with the particles dimensions in any of both cases, it can be easily concluded that the particles were not single crystals but they were formed by the aggregation of small subunits. This fact will be analyzed in more detail later in this paper.

FTIR spectroscopy was used to gain additional information on the samples composition. The spectra of both types of LuF_3 particles (Figure 3, bottom) are very similar to each other and exhibit the absorptions associated with fluoride ions (< 1000 cm^{-1}), along with broad bands at about 3400 cm^{-1} and 1640 cm^{-1} due to absorbed water. The weak features in the 1500-1300 cm^{-1} region are due to carbonate anions coming from the adsorption of atmospheric CO_2. Since no additional impurities could be observed in the FTIR spectra of the samples, the presence of EG species on the particles surface, previously observed for other Ln-doped particles prepared in EG (Singh et al. 2012), can be discarded.

2. Influence of the synthesis conditions on the morphology of the precipitated particles.

The set of experimental conditions mentioned above is essential to obtain uniform LuF_3 particles. The conditions for the synthesis of the LuF_3 rhombus- and cocoon-like particles were so restrictive that keeping the lutetium source constant (as lutetium acetate or lutetium nitrate) and changing, one by one, each of the other experimental parameters (fluoride source, lutetium concentration, ionic liquid concentration, type of solvent, aging temperature and heating source), led to ill-defined, heterogeneous, aggregated or bigger particles, depending on the parameter changed, as described in detail in Table 1 and observed in Figure 1SI and 2SI.

3. Formation mechanism of the LuF_3 particles

To elucidate the mechanism for the formation of the LuF_3 particles, time-dependent experiments were carried out in the synthesis conditions of the rhombus-like and the cocoon particles. TEM images of the corresponding intermediates are shown in Figures 4a and 4b, respectively. Precipitation of three types of particles, consisting of ribbons,

100 nm elongated particles and tiny ill-defined particles (< 10 nm), was observed in both cases in the first stages of the reaction (10 min). Increasing reaction time (15 min) led to the increase in the size of the elongated particles as well as to the decrease in the number of ribbons and tiny particles, the latter being practically missing in the case of the cocoon series. These facts suggest that the elongated particles were formed by the dissolution of the ribbons and tiny particles followed by re-precipitation. However, it cannot be discarded that the tiny particles served as primary nanobuilding units to reassemble and rearrange in a three-dimensional array to form the elongated particles. In fact, the XRD data described above, point to the latter mechanism. The elongated particles already resembled, at this stage of the reaction (15 min), the final rhombus and cocoon shapes. Finally, while the cocoon particles were fully formed after 30 minutes reaction, the rhombus-like particles needed a much longer reaction time (120 min) to complete formation. This observation suggest that the lutetium acetate salt used for the synthesis of the LuF_3 rhombi acted as capping agent, thus delaying the release of the Lu^{3+} ions and, therefore, the formation of the particles. Such delay was not possible in the case of the $Lu(NO_3)_3$ used for the synthesis of the cocoons, which, consequently, formed faster.

Finally, the XRD patterns registered at each reaction stage (Figure 4c and 4d) indicated that no symmetry change took place with reaction time. The patterns just showed the crystallization of orthorhombic LuF_3, which occurred after 10 minutes of reaction in both cases.

The proposed reaction mechanism can be used to understand the change in the morphological characteristics of the LuF_3 particles precipitated under different experimental conditions, as described in the previous section (Table 1). The ionic strength (given by the reactant concentrations) and the dielectric constant of the solvent (42.5, 37 28.8 for glycerol, ethylene glycol, and butylene glycol respectively, at 25 ºC, respectively) determine the equilibrium between attractive and repulsive forces in a colloidal system, thus controlling the aggregation process (Privman et al. 1999).

4. Synthesis, structural characterization and luminescent properties of Eu^{3+}-doped LuF_3 rhombus and cocoon particles.

Eu^{3+} doping was used, as a proof on concept, to analyze the luminescent properties of the resultant LuF_3 rhombus- and cocoon-like phosphors. The synthesis method used to

obtain the undoped particles was also successfully applied to obtain LuF_3 particles of both morphologies doped with Eu^{3+}. Different doping levels were used to evaluate the effect of the Eu^{3+} content on the luminescent properties of the phosphors. Nominal concentrations were 2.5, 5.0, 10, 20, 30 and 40 mol % Eu^{3+} in LuF_3. It was found that the same shape and crystal symmetry as those of the undoped materials were reproduced for the doped samples for all doping levels in both, the rhombus and cocoon particles. However, a significant decrease in particle size (Table 2) was observed when the doping level increased from 20% to 30% in the case of the rhombus-like particles and from 30% to 40% in the case of the cocoon-like particles (Figure 5). Changes in particle size were observed as well by Li et al. (2008) in their study of lanthanide fluorides LnF_3 (Ln=La to Lu) crystals.

To confirm the presence of Eu^{3+} in the LuF_3 crystal structure, that is, replacing Lu^{3+} in their crystallographic sites, the unit cell volumes corresponding to the Eu-doped LuF_3 rhombus- and cocoon-like particles were calculated by the Rietveld analysis of their XRD patterns (Figure 3SI). The values obtained have been plotted in Figure 6 for both types of particles. The cell volume increased with increasing Eu^{3+} content, in agreement with the bigger ionic radius of Eu^{3+} compared with that of Lu^{3+} (Shannon, 1976). In addition, the increase in unit cell volume was linear, satisfying the Vegard´s law (Vegard, 1921) and indicating, therefore, the formation of a solid solution of Eu^{3+} in LuF_3 for both types of morphologies.

To evaluate the luminescent properties of the Eu^{3+}-doped LuF_3 particles, their excitation spectra were recorded by monitoring the emission of the characteristic $^5D_0$-$^7F_1$ transition of Eu^{3+} at 593 nm. Figure 7a shows the excitation spectrum corresponding to the 10% Eu^{3+}-doped LuF_3 rhombus-like particles. The rest of compositions as well as the Eu-doped LuF_3 cocoon-like particles showed very similar excitation spectra to this one. The spectrum showed a set of sharp and well defined excitation bands, the most intense at 393 nm, which correspond to the f-f electronic transitions characteristic of the Eu^{3+} ions (Yan and Li, 2005) and that have been indexed in the figure.

The emission spectra of the Eu^{3+}-doped LuF_3 rhombus particles (molar % Eu^{3+} from 0.5% to 30%) recorded after excitation at 393 nm, are shown in Figure 7b. All of them showed the emission lines corresponding to the well-known $^5D_0$-^7F_J (J= 0, 1, 2, 3, 4) transitions of Eu^{3+}. The $^5D_0$-$^7F_1$ transition is due to the magnetic dipole transition of

Eu^{3+} ions and it is independent of the symmetry of the Eu^{3+} site. However, the $^5D_0$-$^7F_2$ transition is a forced electric dipole transition, hypersensitive to the site symmetry of the Eu^{3+} ions. The lower intensity of the latter indicates that the Eu^{3+} ions are located at a site with inversion center (Blasse and Grabmaier, 1994; Tanner, 2013), in agreement with the orthorhombic *Pnma* structure of LuF_3 (PDF ICDD 00-32-0612). The emission spectra of the Eu^{3+}-doped LuF_3 cocoon particles showed the same emission lines and relative intensities as the previously described for the rhombus-like particles (Figure 4SI). The Eu crystallographic site in the unit cell of the cocoon-like Eu-LuF_3 particles is therefore the same as that of the rhombus like particles described above. It is noteworthy, however, that the intensity ratio (R) of the $^5D_0$-$^7F_2$ transition to the $^5D_0$-$^7F_1$ transition slightly increased with increasing Eu^{3+} content in both types of particles (Table 3). This fact indicates that an increase in the asymmetry of the site occupied by the Eu^{3+} ions takes place as more Lu^{3+} is replaced by Eu^{3+} in the LuF_3 structure. An increase in R has also been reported for other matrices with increasing Eu^{3+} content (Vijayakumar et al. 2014; Kiran, 2014).

As a consequence of the strong intensity of the $^5D_0$-$^7F_1$ transition, the colloidal suspensions of the Eu-doped LuF_3 rhombus- and cocoon-like particles emit a strong orange luminescence under UV radiation with very similar CIE coordinates (x=0.59, x= 0.42 and x= 0.60, y= 0.39, respectively) at any Eu^{3+} content (Figure 7c).

Although the emission spectra of all compositions for both the rhombus-like and cocoon particles are very similar to each other from a qualitative point of view, it can be observed in Figures 7b and 4SI that their absolute intensities vary significantly with increasing Eu^{3+} content. Figure 7d shows the integrated intensity of the emission spectrum obtained for each composition for both, the rhombus-like and cocoon particles. In both cases, the emission intensity increases linearly with increasing Eu^{3+} content, reaching a maximum at the LuF_3:20% Eu^{3+} composition in the case of the rhombus-like particles, and at the LuF_3:30% Eu^{3+} composition in the case of the cocoon particles. The observed increase in luminescence intensity is clearly due to the progressive increase of emission centers as the doping concentration increases. After reaching a maximum, the luminescence intensity decreases with increasing the Eu^{3+} doping level. This fact is generally assigned to the well-known concentration quenching effect, which consists in the energy transfer between adjacent luminescent centers (Yan and Li, 2005; Pi et al. 2005; Cui et al. 2006) and becomes significant when the Eu-Eu

distance decreases as a result of the increase in doping level. However, in our case, the Eu^{3+} concentration at which the luminescence quenches exactly coincides with the size decrease observed in both types of particles (Table 2). It is very likely, therefore, that these two latter facts are related and contribute, together with the concentration quenching effect, to the observed intensity decrease. In fact, any decrease in particle size entails an increase in the surface/bulk ratio with the consequent increase in the number of surface defects that can act as quencher centers of the luminescence.

Conclusions

We have synthesized uniform orthorhombic LuF_3 particles with rhombus-like shape using a very simple method consisting in the aging, at 120ºC for 2 h, a solution containing lutetium acetate (0.02 M) and an ionic liquid of $[BMIM]BF_4$ (0.5 mL) in ethylene glycol (total volume 10 mL). The particles exhibited a rhombus-like morphology with a long axis of ~180-200 nm and a short axis of ~100 nm. Replacing the lutetium acetate by lutetium nitrate also led to uniform LuF_3 particles exhibiting, in this case, a cocoon-like morphology with a long axis of ~300 nm and a short axis of ~150 nm. It was found that the set of experimental conditions mentioned above was essential to obtain uniform LuF_3 particles, as the change of any experimental parameter, keeping the rest constant, only led to ill-defined, heterogeneous, aggregated or bigger particles, depending on the parameter changed. The synthesis method described above was also successfully applied for the synthesis of Eu^{3+}-doped LuF_3 particles of both morphologies. It was found that the crystal structure and shape of the undoped materials were reproduced at any of the Eu^{3+} doping levels used (up to 40%). However, a drastic decrease in size was observed in the rhombus- and cocoon-like particles when 30% and 40% Eu, respectively, was introduced in the LuF_3 structure. Finally, the emission spectra of the different Eu:LuF_3 particles suggested that the highest luminescence intensity was reached at 20% Eu and 30% Eu contents in the rhombus- and cocoon-like particles, respectively. These experimental observations make these materials suitable phosphors for optoelectronic as well as in-vitro biotechonological applications.

Acknowledgements

Supported by MEC (Project. MAT2012-34919), Junta de Andalucía (JA FQM 06090) and CSIC (201460E005).

References

Blasse G, Grabmaier BC (1994) Luminescent Materials. Springer Verlag. Berlin.

Carniato F, Thangavel K, Tei L, Botta M (2013) Structure and dynamics of the hydration shells of citrate-coated GdF_3 nanoparticles. J Mater. Chem. B 1:2442-2446.

Cui Y, Fan X, Hong Z, Wang M (2006) Synthesis and luminescence properties of lanthanide (III)-doped YF_3 nanoparticles. J Nanosci. Nanotech. 6:830-836.

Diamente PR, Raudsepp M, van Veggel FCJM (2007) Dispersible Tm^{3+}-doped nanoparticles that exhibit strong 1.47 μm photoluminescence. Adv. Func. Mater. 17:363-368.

Downing E, Hesselink L, Ralston J, Macfarlane R (1996) A three-color, solid-state, three-dimensional display. Science 273:1185-1189.

Feldmann C (2003) Polyol-mediated synthesis of nanoscale functional materials. Adv Funct Mater 13:101-107.

Jacob DS, Bitton L, Grinblat J, Felner I, Koltypin Y, Gedanken A (2006) Are ionic liquids really a boon for the synthesis of inorganic materials? A general method for the fabrication of nanosized metal fluorides. Chem. Mater. 18**:**3162-3168.

Kiran N (2014) Eu3+ ion doped sodium-lead borophosphate glasses for red light emission J. Mol. Str. 93:1065-1066.

Li C, Yang J, Yang P, Lian H, Lin J (2008) Hydrothermal synthesis of lanthanide fluorides LnF_3 (Ln = La to Lu) nano-/microcrystals with multiform structures and morphologies. Chem. Mater. 20:4317-4326.

Li C, Quan Z, Yang P, Huang S, Lian H, Lin J (2008) Shape-controllable synthesis and upconversion properties of lutetium fluoride (doped with Yb^{3+}/Er^{3+}) microcrystals by hydrothermal process. J. Phys. Chem. C 112:13395-13404.

Li YP, Zhang JH, Luo YS, Zhang X, Hao ZD, Wang XJ (2011) Color control and white light generation of upconversion luminescence by operating dopant concentrations and pump densities in Yb^{3+}, Er^{3+} and Tm^{3+} tri-doped Lu_2O_3 nanocrystals. J. Mater. Chem. 21:2895-2900.

Lin J, Huo J, Cai Y, Wang Q (2013) Controllable synthesis of Eu^{3+}/Tb^{3+} activated lutetium fluorides nanocrystals and their photophysical properties. J Lumin. 144:1-5.

Liu Q, Sun Y, Yang TS, Feng W, Li CG, Li FY (2011) Sub-10 nm Hexagonal Lanthanide-Doped NaLuF4 Upconversion Nanocrystals for Sensitive Bioimaging in Vivo. J. Am. Chem. Soc. 133:17122-17125.

Mai HX, Zhang YW, Si R, Yan ZG, Sun LD, You LP, Yan CH (2006) High-quality sodium rare-earth fluoride nanocrystals: Controlled synthesis and optical properties. J. Am. Chem. Soc. 128:6426-6436.

Matijevic E (1993) Preparation and properties of uniform size colloids. Chem. Mater. 5:412-426.

Maunier C, Doualan JL, Moncorge R, Cavalli E (2002) Growth, spectroscopic characterization, and laser performance of Nd:$LuVO_4$, a new infrared laser material that is suitable for diode pumping. J. Opt. Soc. Am. B 19:1794-1800.

Pi D, Wang F, Fan X, Wang M, Zhang Y (2005) Luminescence behavior of Eu^{3+} doped LaF_3 nanoparticles. Spectrochim. Acta Part A 61:2455-2459.

Privman V, Goia DV, Park J, Matijević E (1999) Mechanism of formation of monodisperse colloids by aggregation of nanosize precursors. J Colloid Interface Sci. 213:36-45.

Qiu P, Zhou N, Wang Y, Zhang C, Wang Q, Sun R, Gao G, Cui D (2014) Tuning lanthanide ion-doped upconversion nanocrystals with different shapes via a one-pot cationic surfactant-assisted hydrothermal strategy. CrystEngComm. 16:1859-1863.

Rao L, Lu W, Ren G, Wang H, Yi Z, Liu H, Zeng S (2014) Monodisperse LaF_3 nanocrystals: shape-controllable synthesis, excitation-power-dependent multi-color tuning and intense near-infrared upconversion emission. Nanotechnology 25:065703.

Shannon RD (1976) Revised effective ionic-radii and systematic studies of interatomic distances in halides and chalcogenides. Acta Cryst. A 32:751-767.

Singh NS, Ningthoujam RS, Phaomei G, Dorendrajit S, Vinu A, Vatsa RK (2012) Re-dispersion and film formation of $GdVO_4$: Ln^{3+} (Ln^{3+} = Dy^{3+}, Eu^{3+}, Sm^{3+}, Tm^{3+}) nanoparticles: particle size and luminescence studies. Dalton Trans. 41:4404-4412.

Sudesh V, Asai K (2003) Spectroscopic and diode-pumped-laser properties of Tm,Ho: YLF; Tm,Ho:LuLF; and Tm,Ho:LuAG crystals: a comparative study. J. Opt. Soc. Am. B 20:1829-1837.

Sun YJ, Chen Y, Tian LJ, Yu Y, Kong XG, Zhao JW, Zhang H (2007) Controlled synthesis and morphology dependent upconversion luminescence of NaYF4 : Yb, Er nanocrystals. Nanotechnology 18:275609.

Tanner PA (2013) Some misconceptions concerning the electronic spectra of tri-positive europium and cerium. Chem. Soc. Rev. 42:5090-5101.

Vegard L (1921) The constitution of the mixed crystals and the filling of space of the atoms. Z. fur Physik 5:17-26.

Vijayakumar R, Maheshvaran K, Sudarsan V, Marimuthu K (2014) Concentration dependent luminescence studies on Eu^{3+} doped telluro fluoroborate glasses. J. Lumin. 154:160-167.

Wang LY, Li YD (2006) Green upconversion nanocrystals for DNA detection. Chem Comm. 24:2557-2559.

Wang L, Li Y (2007) Controlled synthesis and luminescence of lanthanide doped $NaYF_4$ nanocrystals. Chem. Mater. 19:727-731.

Xiao S, Yang X, Ding JW, Yan XH (2007) Up-conversion in Yb^{3+}-Tm^{3+}Co-doped lutetium fluoride particles prepared by a combustion-fluorization method. J. Phys. Chem. C 111:8161-8165.

Yan R, Li Y (2005) Down/Up conversion in Ln^{3+}-doped YF_3 nanocrystals. Adv. Funct. Mater. 15:763-770.

Yi GH, Lu HC, Zhao SY, Yue G, Yang WJ, Chen DP, Guo LH (2004) Synthesis, characterization, and biological application of size-controlled nanocrystalline $NaYF_4$: Yb,Er infrared-to-visible up-conversion phosphors. Nano lett. 4:2191-2196.

Table 1: Morphology of the particles obtained after changing one of the parameters used to synthesize the LuF_3 rhombus- and cocoon-like particles (given in Figure 1), keeping the other parameters constant.

Parameter	Value	Rhombus experimental conditions	Ovoid experimental conditions
Lutetium source	Lutetium acetilacetonate	Big, irregular particles	
Lutetium concentration	0.005	Ill-defined rhombi	Ovoid particles (400 nm long axis)
	0.03		Elongated particles (~400 nm long axis)
Fluoride source	$NaBF_4$	Ill-defined particles	Ovoid particles (500 nm long axis)
	NH_4F	Rounded particles with two different sizes (~300 nm and ~30 nm)	Agglomerated particles
([BMIM]BF_4) volumen (cm^3)	0.25	Rhombi with high particle size distribution	Heterogeneous particles
	1.0	Ill-defined particles	Ill-defined particles
Solvents	Glycerol	Rounded particles with two different sizes (~60 nm and ~10 nm)	Agglomerated nanoparticles
	Buthylene Glicol	Insoluble	Ill-defined particles
	Dietylene Glycol	Insoluble	Ill-defined particles
Aging temperatura (ºC)	180	Heterogeneous rhombus-like particles	Heterogeneous particles
	80	Rise-like particles (300 nm) + nanoparticles (10 nm)	Rounded, agglomerated particles (~100 nm)
Heating source	Microwaves	Rhombus-like particles with two different sizes (~400 nm and ~20 nm)	Heterogeneous particles

Table 2: Dimensions of the Eu:LuF_3 rhombus- and cocoon-like particles at different Eu^{3+} doping levels.

Type of LuF_3 particle	Molar % Eu^{3+}	Long axis length (nm)	Short axis length (nm)
Rhombi	0-20	200	100
	30	120	60
Cocoons	0-30	300	150
	40	120	80

Table 3: Asymmetry ratio (R) of the $^5D_0$-$^7F_2$ transition to the $^5D_0$-$^7F_1$ transition as a function of Eu^{3+} content.

Molar % Eu^{3+}	R (Rhombi)	R (Cocoons)
10	0.22	0.26
20	0.26	0.28
30	0.31	0.28
40	0.33	0.36

FIGURE CAPTIONS

Figure 1: TEM micrographs of the LuF_3 particles synthesized after aging at 120 ºC a solution containing lutetium acetate (a) and lutetium nitrate (b) and $[BMIM]BF_4$ in ethylene glycol. Aging time: 2h and 30 min in a and b, respectively. The insets show a magnified image particle of each particle type.

Figure 2: Size distribution of the two types of particles shown in Figure 1 calculated by Dynamic Light Scattering.

Figure 3: *Top:* XRD patterns of the two types of particles shown in Figure 1. The PDF file shown at the bottom corresponds to orthorhombic LuF_3. *Bottom:* FTIR spectra of both types of particles.

Figure 4: a and b) TEM micrographs of three different intermediates in the formation of the rhombus- and cocoon-like LuF_3 particles. c and d) XRD patterns corresponding to the intermediates shown in a and b, respectively.

Figure 5: TEM micrographs of the Eu^{3+}-doped LuF_3 rhombus- (top) and cocoon- (bottom) like particles with different Eu contents.

Figure 6: Unit cell volume of the Eu:LuF_3 rhombus- and cocoon-like particles as a function of Eu^{3+} concentration calculated by the Rietveld analysis of their corresponding XRD patterns (the latter shown in Figure 3SI). The error bars are approximately the size of the symbols.

Figure 7: a) Excitation spectrum of the 5%Eu-doped LuF_3 rhombus-like particles recorded at the emission wavelength of 588 nm. b) Emission spectra of different Eu-containing LuF_3 rhombus like particles recorded at an excitation wavelength of 394 nm. c) CIE diagram showing the chromatic coordinates of the rhombus- (square) and cocoon- (circle) like Eu:LuF_3 particles. d) Integrated area of the emission spectra of the rhombus- and cocoon-like Eu:LuF_3 particles as a function of Eu^{3+} concentration.

Figure 1

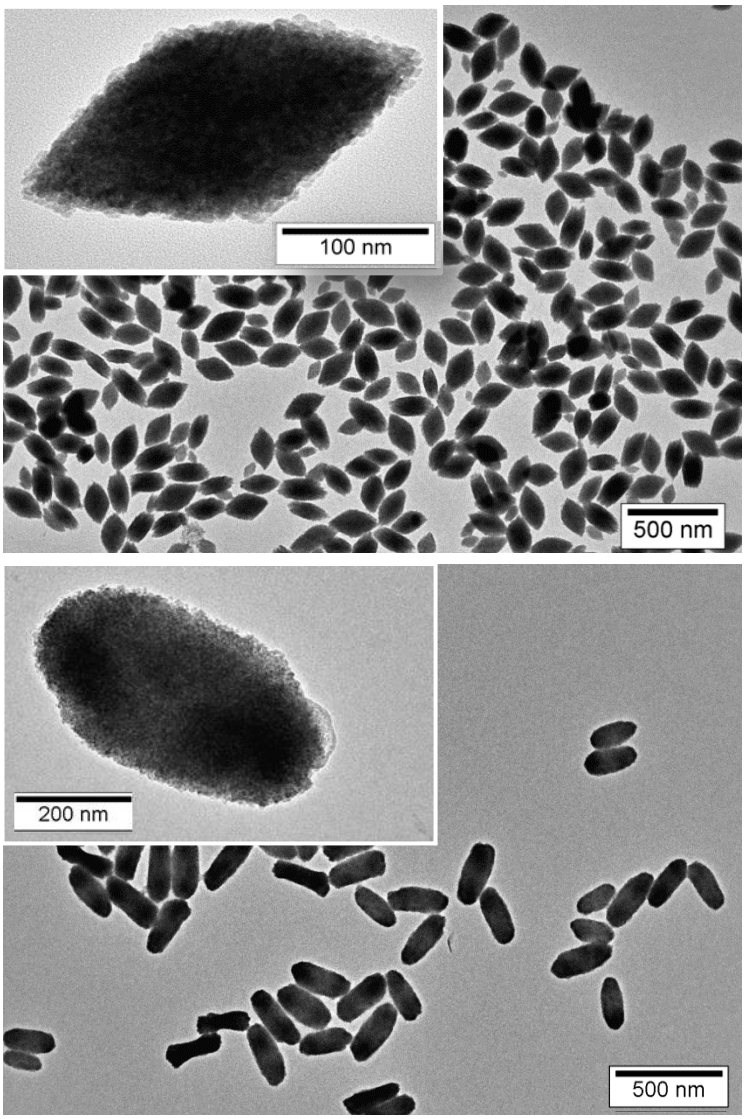

Figure 2

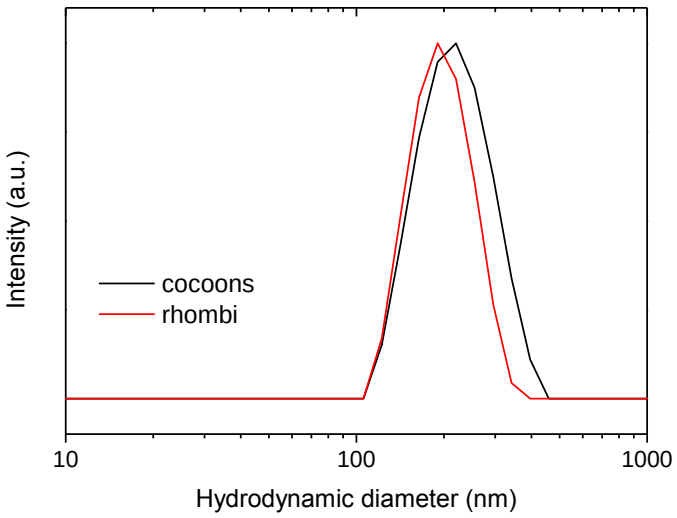
Intensity (a.u.)
cocoons
rhombi
10
100
1000
Hydrodynamic diameter (nm)

Figure 3

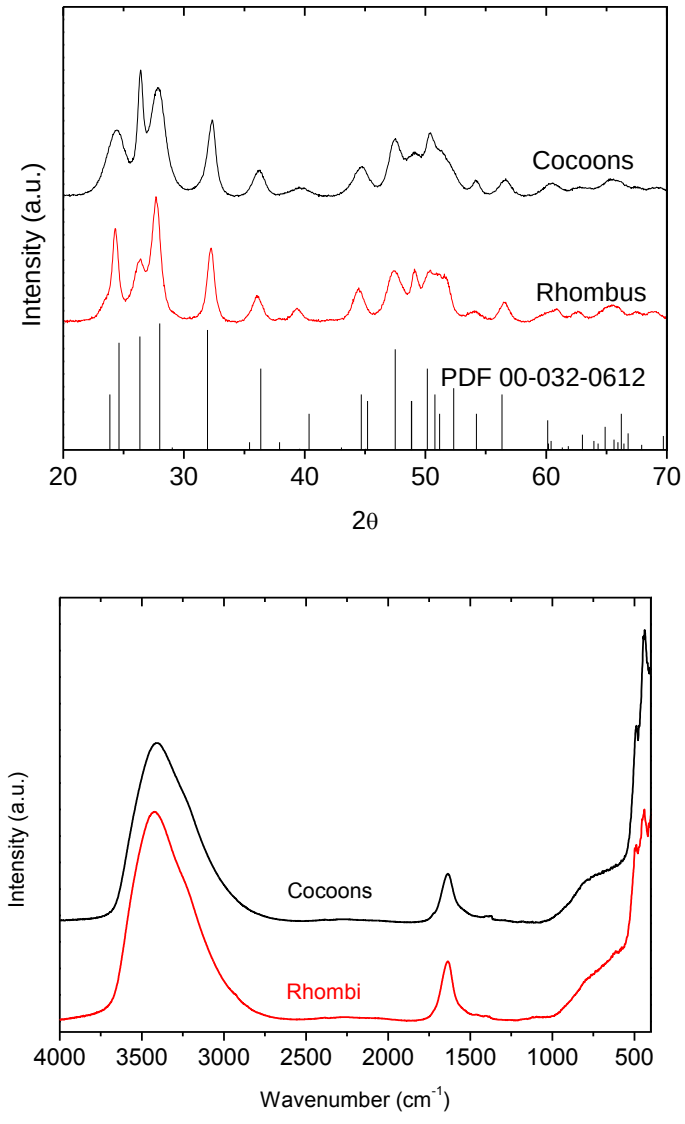
Intensity (a.u.)
Cocoons
Rhombus
PDF 00-032-0612
20
30
40
50
60
70
2θ
Intensity (a.u.)
Cocoons
Rhombi
4000
3500
3000
2500
2000
1500
1000
500
Wavenumber (cm-1)

Figure 4

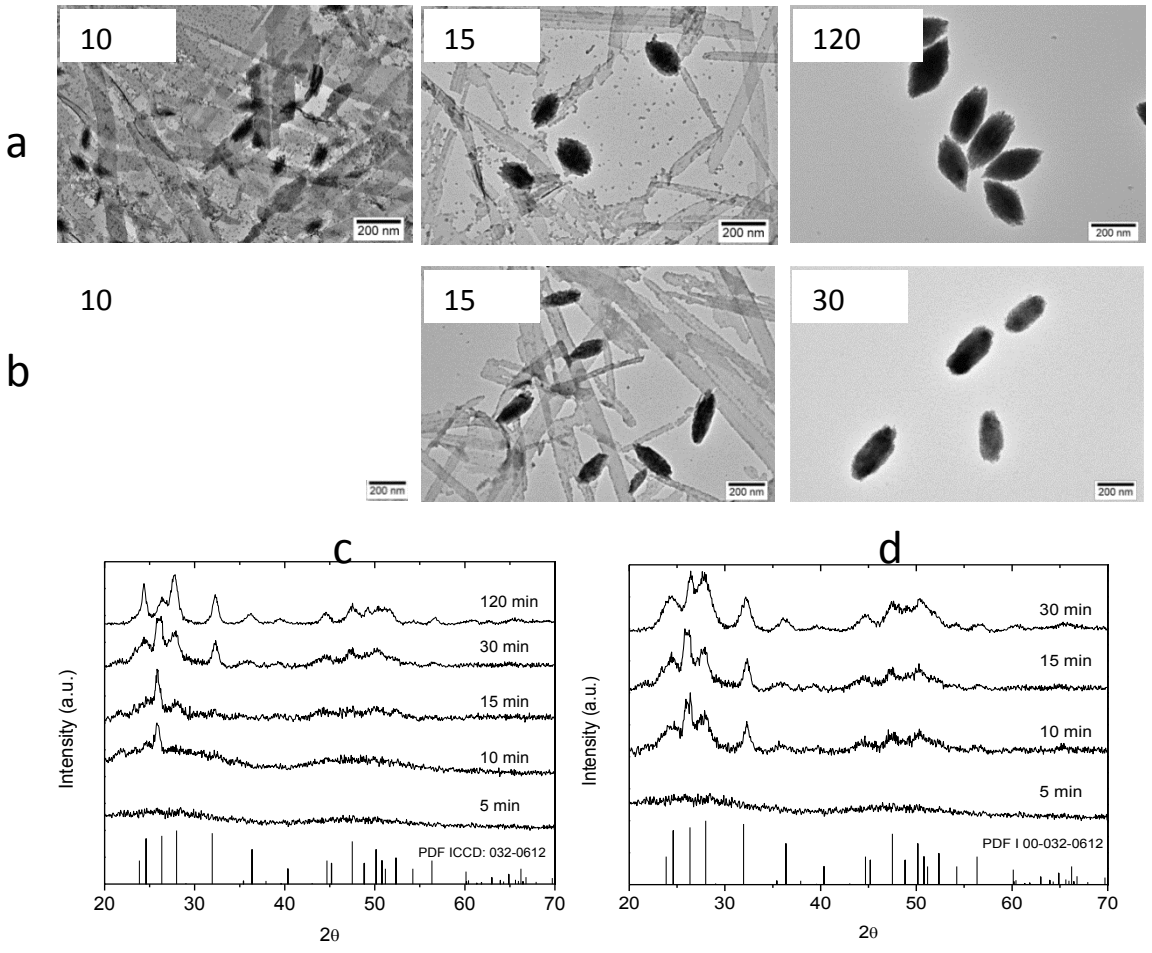
a
10
15
120
200 nm
b
10
15
30
200 nm
c
120 min
30 min
15 min
10 min
5 min
PDF ICCD: 032-0612
Intensity (a.u.)
20
30
40
50
60
70
2θ
d
30 min
15 min
10 min
5 min
PDF I 00-032-0612
Intensity (a.u.)
20
30
40
50
60
70
2θ

Figure 5

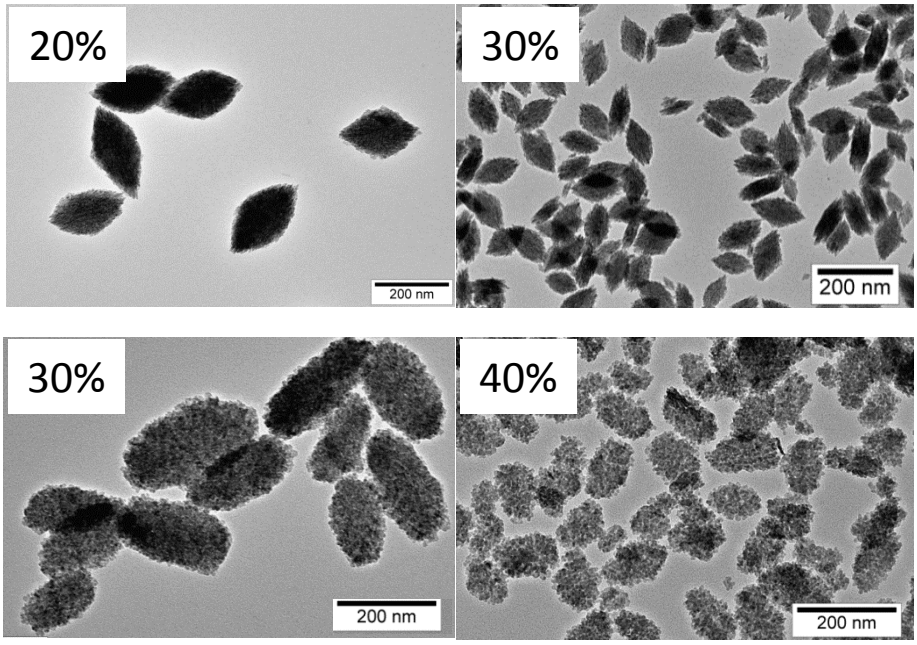

Figure 6

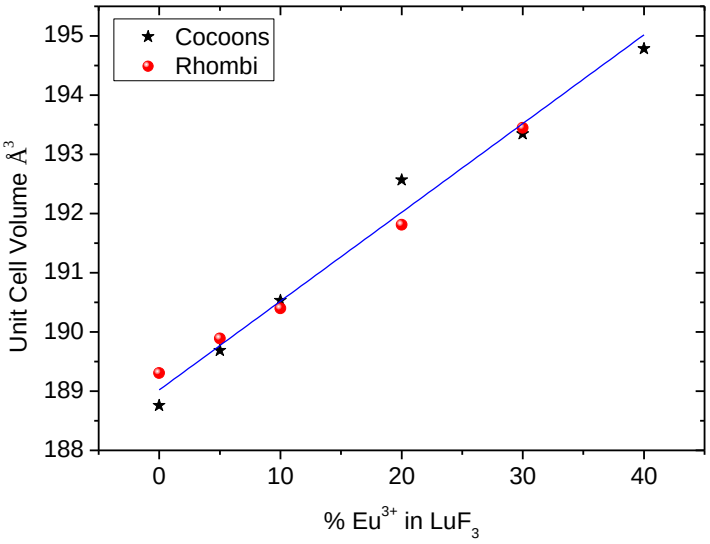
Cocoons
Rhombi
Unit Cell Volume Å^3
% Eu^{3+} in LuF$_3$
195
194
193
192
191
190
189
188
0
10
20
30
40

Figure 7

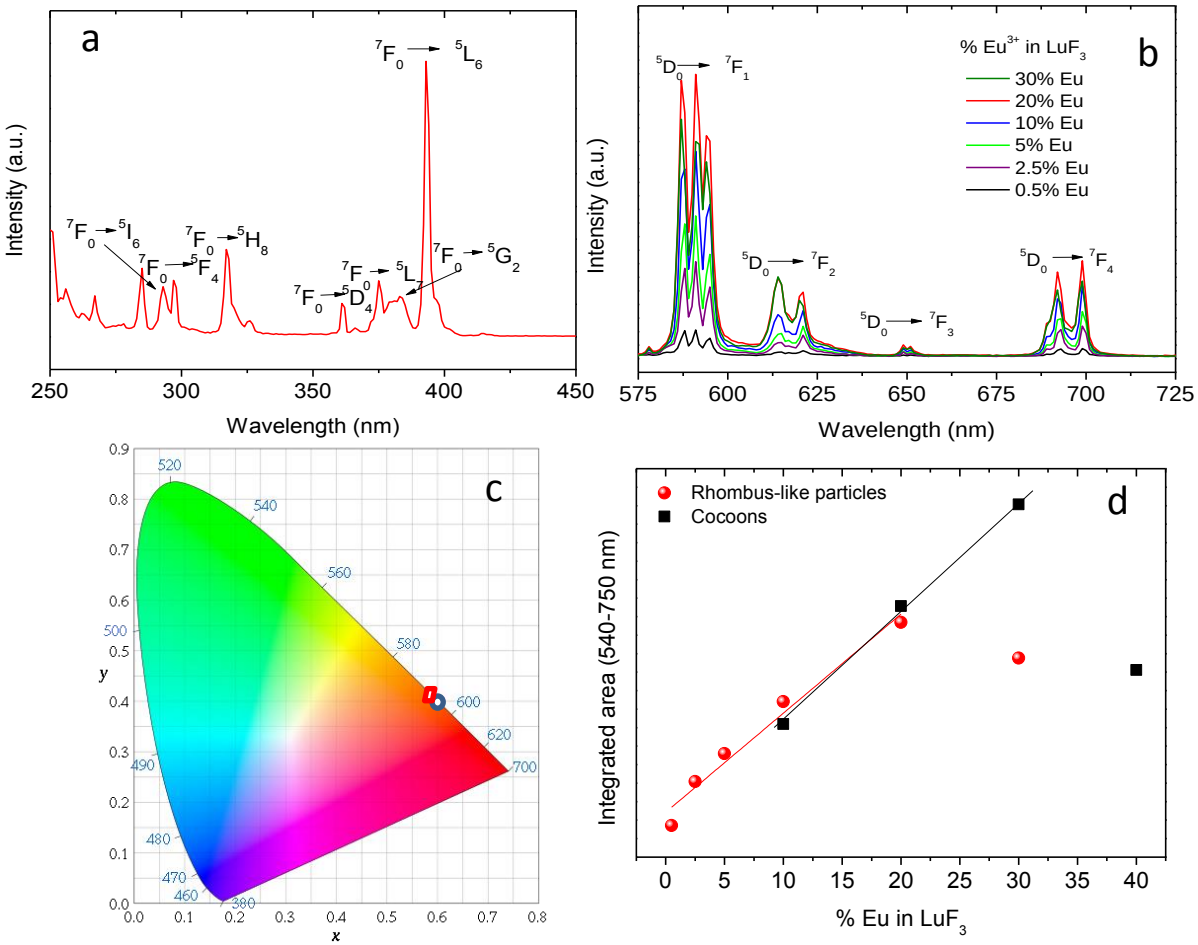
a
Intensity (a.u.)
Wavelength (nm)
$^7F_0 \rightarrow {}^5L_6$
$^7F_0 \rightarrow {}^5I_6$
$^7F_0 \rightarrow {}^5H_8$
$^7F_0 \rightarrow {}^5F_4$
$^7F_0 \rightarrow {}^5L_7$
$^7F_0 \rightarrow {}^5D_4$
$^7F_0 \rightarrow {}^5G_2$
b
% Eu^{3+} in LuF_3
30% Eu
20% Eu
10% Eu
5% Eu
2.5% Eu
0.5% Eu
$^5D_0 \rightarrow {}^7F_1$
$^5D_0 \rightarrow {}^7F_2$
$^5D_0 \rightarrow {}^7F_3$
$^5D_0 \rightarrow {}^7F_4$
c
x
y
d
Rhombus-like particles
Cocoons
Integrated area (540-750 nm)
% Eu in LuF_3